Check for updates

Unveiling the reactivity of CO_2 with carbanions: a theoretical analysis of the carboxylation step†

Catia Nicoletti, [ID] * Manuel Orlandi, [ID] Luca Dell'Amico [ID] and Andrea Sartorel [ID] *

The synthetic insertion of carbon dioxide into organic scaffolds typically requires the reaction of CO_2 with a carbanion (carboxylation step), with the latter being generated through chemical, electrochemical, or photochemical routes. Still, little is known about the energetic and structural requirements of this step. In this work, we unveil the reactivity of CO_2 with a selected set of 28 carbanions through DFT calculations and provide linear free-energy relationships that correlate the ΔG^0 and the $\Delta G^{\ddagger}$ of the carboxylation step. These reveal a Leffler–Hammond parameter $\alpha = 0.26 \pm 0.02$ and an intrinsic barrier $\Delta G_0^{\ddagger} = 12.7 \pm 0.3$ kcal mol^{-1} (ωb97XD/aug-cc-pvtz//ωb97XD/def2tzvp level of theory), indicative of smooth reactivity of carbanions with CO_2. This reactivity is further associated with the basicity of the carbanions (expressed as the pK_{aH} of the conjugate acid), in a linear Brønsted plot between calculated $\Delta G^{\ddagger}$ and experimental pK_{aH} (slope $\beta = 0.40 \pm 0.04$ kcal mol^{-1}). According to the Mayr–Patz equation, calculations allow the extrapolation of electrophilicity values for CO_2 in the range from -15.3 to -18.7, in good agreement with a single reported experimental value of -16.3. Concerning the structural changes occurring in the transition state, the major energy penalty comes from the distortion of CO_2. These findings can be useful in designing novel reactivity targeting carbon dioxide fixation.

Introduction

Carbon dioxide is a by-product of many anthropogenic activities, and its current increase in the atmosphere is causing severe climate changes.[1] On the other hand, CO_2 is a cheap, non-toxic and renewable single carbon atom building block that can be exploited for fuel production or for organic synthesis. Strategies to capture and reconvert CO_2 into fuels or chemicals are thus important targets for achieving carbon neutrality,[2] in line with the United Nations sustainable development goals.[3] Current carbon dioxide capturing technologies exploit amine solutions, with the formation of carbamate salts;[4,5] CO_2 is then released by an energy demanding thermal step involving heating of the solution up to 100–125 °C. Electrochemical methods are considered as possible alternatives to avoid the need for an external high temperature energy source; they can operate through electrochemically induced displacement reactions (such as in the case of electrochemically modulated amine regeneration) or through CO_2 binding to electrochemically reduced nucleophilic capturing agents, such as quinones.[4,6]

Concerning carbon dioxide reconversion, some strategies target CO_2 reduction to C_1 or C_{2+} products.[7–9] For instance, a cobalt phthalocyanine molecular catalyst was exploited to mediate CO_2 to CO formation in a zero-gap membrane flow reactor with selectivity >95% at an impressive current density of 150 mA cm^{-2}.[10] Examples of reduction of CO_2 to C_2 products include the use of a 3D dendritic copper–cuprous oxide composite for acetic acid and ethanol production[11] and the use of single site metal catalysts. In this field, the use of DFT calculations for a thermodynamic and kinetic analysis of the relevant steps is considered a powerful tool for catalyst design.[8,12]

Finally, carbon dioxide is a single carbon atom building block to be exploited in organic synthesis.[13–18] In this regard, processes involving CO_2 are already industrialised for the preparation of linear and cyclic carbonates (from alkynes or epoxides), for urea synthesis,[19] and in the Kolbe–Schmitt reaction[20,21] for the preparation of salicylic acid and 3-hydroxy-2-naphthoic acid (from sodium phenolate and 2-naphtholate, respectively).

CO_2 is however a thermodynamic sink of the carbon cycle and its conversion requires highly reactive chemicals, transition metal catalysis[22,23] and/or severe reaction conditions.[13,24] An appealing strategy is the formation of new C–C bonds through the polar reaction of CO_2 with nucleophilic carbanions generated through chemical,[25,26] electrochemical,[27,28] or photochemical routes.[29–31] This strategy enabled the preparation of products of pharmaceutical interest – although obtained as racemic mixtures – such as amino acids,[32,33] the anti-epilepsy and absence seizure drug ethosuximide precursor (synthesised *via* electrochemical hydrocarboxylation in flow),[34] and

Department of Chemical Sciences, University of Padova, via Marzolo 1, 35131 Padova, Italy. E-mail: Catia.nicoletti@phd.unipd.it; Andrea.sartorel@unipd.it

† Electronic supplementary information (ESI) available: Details of calculations and additional tables and figures. See DOI: https://doi.org/10.1039/d4se01065e

benzylic carboxylic acids such as fenoprofen, flurbiprofen, ibuprofen and naproxen.[35]

However, while earlier reports rationalised the conversion of CO_2 to formate using metal and organic hydrides,[36] its reactivity with carbanion nucleophiles is still poorly understood, due to very limited kinetic data available.[37] In a seminal work by Ofial and Mayr, a rate constant for the carboxylation step was reported only for the indenide anion (bimolecular $k = 2.09 \pm 0.07$ 10^5 M^{-1} s^{-1}, in dimethylsulfoxide at 20 °C).[37] Therefore, the rationalisation of the thermodynamic, kinetic and structural requirements that govern the reactivity of carbanions with CO_2 is an important target, from the perspective of designing novel carboxylation processes. In particular, the prediction of free energy barriers and reaction rates on the basis of physical parameters of carbanions would be a powerful tool for an *a priori* evaluation of the envisaged reactivity.

In this work, we sought to unveil the reactivity of CO_2 with carbanions by exploiting DFT calculations. We thus considered a selected set of 28 organic carbanions ($\mathbf{R}_i^-$) and calculated both the standard free energy (ΔG^0) and the activation free energy ($\Delta G^\ddagger$) of the carboxylation step (eqn (1) and Scheme 1). Products and transition states will be denoted as $\mathbf{R}_i\text{-COO}^-$ and $\mathbf{R}_i\text{-TS}$, respectively.

$$\mathbf{R}_i^- + CO_2 \rightleftharpoons \mathbf{R}_i\text{-COO}^- \quad \Delta G^0, \Delta G^\ddagger \qquad (1)$$

We will show that ΔG^0 and $\Delta G^\ddagger$ correlate in linear free-energy relationships (also known as rate-equilibrium relationships[38]), whose slope α provides the Leffler–Hammond parameter (describing the fraction of the change in the Gibbs energy of the reaction reflected in the change of the Gibbs energy of activation[39]) and the intercept $\Delta G_0^\ddagger$ is the intrinsic barrier (*i.e.* the activation free energy for an isoergonic reaction). Compared to other organic reactions, these parameters indicate low $\Delta G^\ddagger$ for the carboxylation step with a slight dependence on ΔG^0, identifying CO_2 as a powerful electrophile. The reactivity of the carbanions in terms of $\Delta G^\ddagger$ correlates with their basicity, in a Brønsted plot. Distortion/interaction analysis using the model developed by Bickelhaupt and Houk groups[40] reveals that the carboxylation step is controlled by both carbanion/CO_2 interaction and distortion of the reactants. The interaction is correlated to the basicity of the carbanion; concerning the distortion, the most important contribution to the activation

energy penalty is made by the distortion of CO_2, in terms of the reduction of the O–C–O angle and the $C(\mathbf{R}_i^-)\cdots C(CO_2)$ distance in the transition states. Both these geometric parameters linearly correlate indeed with $\Delta G^\ddagger$.

Computational methods

Calculations were performed with Gaussian16 software.[41] Most carbanions included in this study possess few rotatable bonds. In the cases of anions with possible multiple conformations that may impact the target C-site reactivity (*i.e.* anions $\mathbf{R}_{23}^-$, $\mathbf{R}_{24}^-$, $\mathbf{R}_{25}^-$, and $\mathbf{R}_{27}^{2-}$), an initial conformational search was performed with a semiempirical pm3 method[42–44] including a solvation model for acetonitrile to identify the most stable conformers that were then optimized with DFT methods (see ESI, Fig. S1–S4†). In the manuscript and in the correlations presented, we report $\Delta G^\ddagger$ and ΔG^0 data for the most stable conformer of these anions. We have corroborated this assumption by performing calculations and analysing the $\Delta G^\ddagger$ and ΔG^0 data also for the second most stable conformer of $\mathbf{R}_{23}^-$, $\mathbf{R}_{24}^-$ and $\mathbf{R}_{25}^-$. From the results reported in Table S1 in the ESI,† the variations of the calculated activation and standard free energy of carboxylation resulting from changes in the nature of the initial conformer are in a range of 0.16–0.65 and 0.73–2.14 kcal mol^{-1}, respectively, minimally impacting the correlations presented in this work.

Structures were optimized with DFT methods including a continuum solvation model for acetonitrile (or dimethylsulfoxide) using the integral equation formalism variant (IEFPCM).[45–47] Analysis of the frequencies was performed to assess the nature of the stationary points; in particular, for the transition states, the presence of a single imaginary frequency was confirmed, and the reliability of the transition states was corroborated by intrinsic reaction coordinate (IRC) analysis. For all calculations, a pruned (99 590) integration grid was used. For all the species, a correction of +1.90 kcal mol^{-1} was applied to the computed free energy values to convert the standard state from 1 atmosphere to a 1 M solution.[37,48] When specified, corrections for entropy were applied according to the Truhlar model,[49] using a frequency cut-off value of 100.0 wavenumber.

The following levels of theory were employed:

ωb97XD/def2tzvp//ωb97XD/def2tzvp: geometries optimised using the ωb97XD[50] hybrid functional taking advantage of Grimme's dispersion model with Ahlrichs' triple-zeta basis set def2tzvp;[51,52]

ωb97XD/aug-cc-pvtz//ωb97XD/def2tzvp: geometries optimized at the ωb97XD/def2tzvp level, followed by a single point energy calculation performed using the same functional and the aug-cc-pvtz basis set[53,54] including diffuse functions;

b2plypd/aug-cc-pvtz//ωb97XD/def2tzvp: geometries optimized at the ωb97XD/def2tzvp level, followed by a single point energy calculation performed using the double hybrid b2plypd functional,[55] with the aug-cc-pvtz basis set;

b3lyp/6–311g(d,p)//b3lyp/6–311g(d,p): geometries optimised using the b3lyp functional (without dispersion correction) with a Pople[56] 6–311g(d,p) basis set (not including diffuse functions).
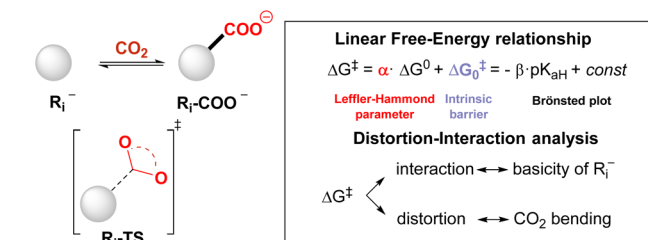
Scheme 1 Schematic representation of the carboxylation step of a carbanion $\mathbf{R}_i^-$ to $\mathbf{R}_i\text{-COO}^-$, and representation of the transition state $\mathbf{R}_i\text{-TS}$. Linear free-energy relationship and distortion–interaction analysis explored in this work.

Results and discussion

Evaluation of the level of theory

The availability of an experimental $\Delta G^{\ddagger}$ value of 10.0 kcal mol^{-1} for the carboxylation of the indenide anion $\mathbf{R_2}^-$ from a bimolecular rate constant of 2.09 ± 0.07 10^5 M^{-1} s^{-1} (in dimethylsulfoxide at 20 °C)[37] allowed the evaluation and the selection of the suitable level of theory among the four levels discussed in the "Computational methods" section. The four levels of theory (continuum model for dimethylsulfoxide solvent) provided calculated $\Delta G^{\ddagger}$ for the carboxylation of $\mathbf{R_2}^-$ in the range 11.9–15.2 kcal mol^{-1}, in good agreement with the experimental value (Table S2 in the ESI†). The best match was found at the ωb97XD/aug-cc-pvtz//ωb97XD/def2tzvp level (calculated $\Delta G^{\ddagger} =$ 11.9 kcal mol^{-1}), which was chosen as the level for the calculations discussed in this work. Corrections for entropy according to the Truhlar model[49] lead to an increase of +0.7 kcal mol^{-1} in the calculated activation free energies and thus were not further applied.

Calculations of ΔG^0 and $\Delta G^{\ddagger}$ for the carboxylation step

The carbanions $\mathbf{R_i}^-$ were selected from our previous investigation,[57] and the corresponding carboxylated species $\mathbf{R_i\text{-}COO}^-$ are represented in Fig. 1. Since several reports exploit acetonitrile as the solvent for carboxylation reactions, this was chosen as the medium for the calculations presented in this work. Fig. 2A reports the plot of $\Delta G^{\ddagger}$ vs. ΔG^0 values for the carboxylation step (ωb97XD/aug-cc-pvtz//ωb97XD/def2tzvp level of theory, including a continuum model for acetonitrile solvent; data including the calculations at the other levels are reported in Tables S3–S7 and Fig. S5 in the ESI†). The geometries of the transition states $\mathbf{R_4\text{-}TS}$ and $\mathbf{R_{17}\text{-}TS}$ are also shown in Fig. 2A as representative cases.
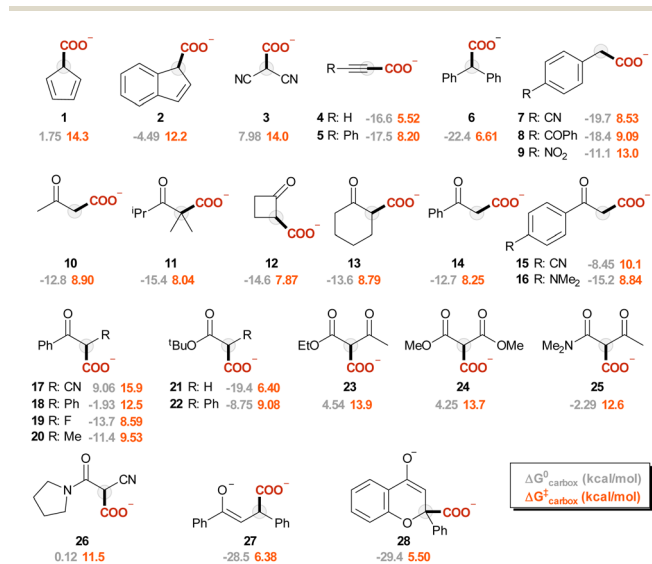
Fig. 1 Representation of $\mathbf{R_i\text{-}COO}^-$ considered in this work (i is indicated below each structure), together with ΔG^0 and $\Delta G^{\ddagger}$ values for the carboxylation step at the ωb97XD/aug-cc-pvtz//ωb97XD/def2tzvp level of theory.
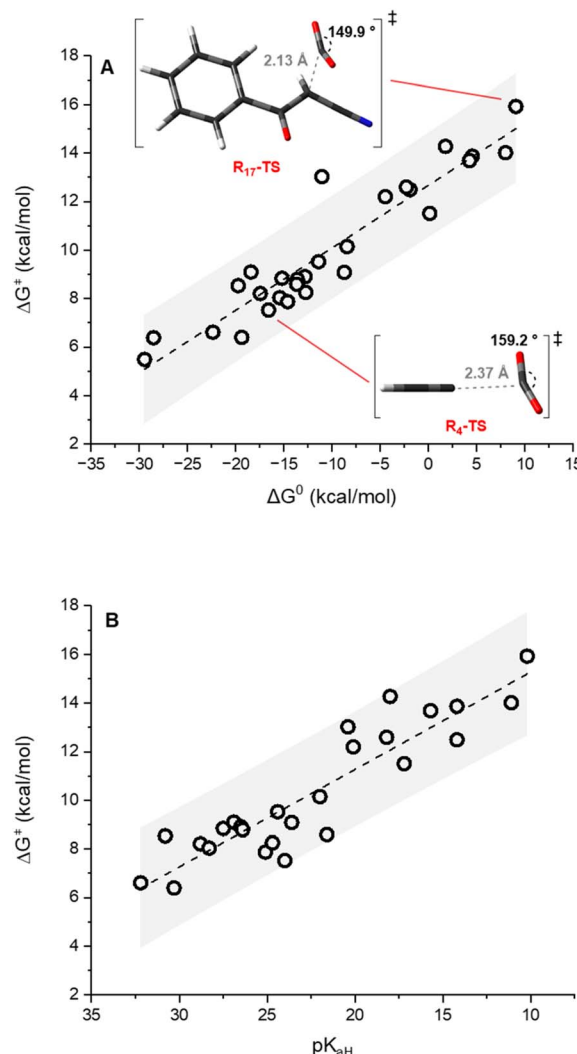
Fig. 2 (A) Plot of $\Delta G^{\ddagger}$ vs. ΔG^0 values for the carboxylation of carbanions $\mathbf{R_i}^-$ (ωb97XD/aug-cc-pvtz//ωb97XD/def2tzvp level of theory, including a continuum model for acetonitrile solvent). The shaded ranges represent the 95% confidence interval of the correlations. Geometries of $\mathbf{R_4\text{-}TS}$ and $\mathbf{R_{17}\text{-}TS}$ (ωb97xd/def2tzvp level) are shown as representative cases of transition states with low and high $\Delta G^{\ddagger}$. (B) Plot of $\Delta G^{\ddagger}$ (ωb97XD/aug-cc-pvtz//ωb97XD/def2tzvp) vs. experimental pK_{aH} of carbanions $\mathbf{R_i}^-$.

Clearly, considering that charged species are involved in eqn (1), solvation impacts the ΔG^0 and $\Delta G^{\ddagger}$ values. While this was addressed by the inclusion of an implicit solvation model, any possible deviation from an ideal explicit solvation could be neglected assuming that such an effect would be similar through the anion series, thus preserving the sought-after linear correlations. Also, the impact of cations possibly present under real reaction conditions could impact the structure and the reactivity of carbanions; this is particularly relevant for the case of enolate like anions in the presence of small alkali cations.[58]

The data plot of $\Delta G^{\ddagger}$ vs. ΔG^0 values shows a good linear trend according to eqn (2) ($R^2 = 0.88$).

$$\Delta G^{\ddagger} = \alpha \times \Delta G^0 + \Delta G_0^{\ddagger} \tag{2}$$

$$\alpha = 0.26 \pm 0.02; \Delta G_0^{\ddagger} = 12.7 \pm 0.3 \text{ kcal mol}^{-1}$$

The slope α of 0.26 ± 0.02 corresponds to the Leffler–Hammond parameter $\alpha = \delta\Delta G^{\ddagger}/\delta\Delta G^0$, describing the fraction of the change in the Gibbs energy of the reaction reflected in the change of the Gibbs energy of activation.[39] It is worth noting that α has long been exploited as an indication of the position of the transition state along the reaction coordinate (with α close to 0 indicating an early transition state and α close to 1 indicating a late transition state), until Bordwell's observation of an α value of 1.31 for the deprotonation of substituted 1-nitro-1-phenylethanes (nitroalkane anomaly)[59] evidenced that the former interpretation was wrong and that α cannot be a measure for the position of the transition state.

The intercept of the fitting in Fig. 2 $\Delta G_0^{\ddagger} = 12.7 \pm 0.3$ kcal mol^{-1} provides the intrinsic barrier, i.e. the activation free energy for an isoergonic reaction (with $\Delta G^0 = 0$).‡ Importantly, quadratic fitting of the data in Fig. 2 according to the Marcus model for group transfer reactions (eqn (3)) leads to consistent values of $\Delta G_0^{\ddagger}$ of 14.2 ± 0.4 kcal mol^{-1}, see ESI Fig. S6.† According to the Marcus model for group transfer in bimolecular reactions, the $\Delta G_0^{\ddagger}$ is associated with the reorganization energy λ ($\lambda = 4 \times \Delta G_0^{\ddagger}$), with λ being estimated to be 50.8 ± 1.2 kcal mol^{-1}.

$$\Delta G^{\ddagger} = \Delta G_0^{\ddagger} + 0.5 \times \Delta G^0 + \{(\Delta G^0)^2/(16 \times \Delta G_0^{\ddagger})\} \quad (3)$$

Comparable α and $\Delta G_0^{\ddagger}$ values were found with the other levels of theory employed (Fig. S5 in the ESI†). Importantly, α and $\Delta G_0^{\ddagger}$ parameters determined from the fittings are in line with those reported for the decarboxylation reaction of organic carboxylates in water (i.e. the microscopically reverse reaction of eqn (1));[60] the value of α reported in this case was 0.76/0.78 (experimental/computed; note that the sum of α for the forward and for the backward step must be 1.00,[39] while the intrinsic barrier was 15.5/16.8 kcal mol^{-1} (experimental/computed).[60] The α and $\Delta G_0^{\ddagger}$ parameters extrapolated from the data in Fig. 2A indicate smooth reactivity of carbanions with CO$_2$,[61] characterised by low energy barriers and by a slight dependence on ΔG^0; these identify CO$_2$ as a powerful electrophile, comparable to carbonyl compounds[37,62] and support the recent observation of the exchange of the COO group from carboxylate salts, occurring under an atmosphere of CO$_2$ at room temperature and in the absence of catalysts.[63,64] As a comparison, in nucleophilic substitutions α values between 0.48 and 0.73 were found for the reaction of several types of nucleophiles with benzhydrylium ions,[39] while the intrinsic barriers $\Delta G_0^{\ddagger}$ reach up to 45 kcal mol^{-1} for carbanion nucleophiles.[65,66] An intrinsic barrier of 14.1 kcal mol^{-1} was reported for the addition of enolate ions to the carbonyl group of

‡ The existence of a linear correlation between $\Delta G^{\ddagger}$ and ΔG^0 is indicative of a constant $\Delta G_0^{\ddagger}$ throughout the reaction series or of a $\Delta G_0^{\ddagger}$ varying proportionally to ΔG^0.

benzaldehyde.[67] Lower intrinsic barriers have been observed for proton and hydride transfer (1–10 kcal mol^{-1}).[68–70]

Four further points are worth mentioning.

(i) We previously reported a linear correlation between variations in ΔG^0 and the change of the basicity of the carbanion $\mathbf{R}_i^-$ expressed as the pK_{aH} of the conjugate acid (eqn (4));[57] combination of eqn (2) and (4) allows the direct correlation of variations in $\Delta G^{\ddagger}$ with pK_{aH}, in a Brønsted type plot (eqn (5)). Indeed, a good linear correlation of calculated $\Delta G^{\ddagger}$ with experimental pK_{aH}[71] is observed in Fig. 2B ($R^2 = 0.83$), providing a powerful prediction tool of $\Delta G^{\ddagger}$.

$$\delta(\Delta G^0) = -1.30 \text{ kcal mol}^{-1} \times \delta(\text{p}K_{aH}) \quad (4)$$

$$\Delta G^{\ddagger} = -\beta \times \text{p}K_{aH} + \text{const} \quad (5)$$

with $\beta = 0.40 \pm 0.04$ kcal mol^{-1} and const = 19.3 ± 0.9 kcal mol^{-1}.

(ii) The calculated $\Delta G^{\ddagger}$ values can be exploited to contextualise the carboxylation step on a more general nucleophilic/electrophilic scale, exploiting the Mayr–Patz equation (eqn (6)),[72]

$$\log k \ (20 \ ^{\circ}\text{C}) = s_N(N + E) \quad (6)$$

where k (20 °C) is the reaction rate constant at 20 °C, N is the nucleophilicity parameter, E is the electrophilicity parameter, and s_N is a nucleophile-specific sensitivity parameter. By obtaining $\log k$ (20 °C) from $\Delta G^{\ddagger}$ through the Eyring equation and exploiting the reported S_N and N parameters for carbanions $\mathbf{R}_2^-$, $\mathbf{R}_3^-$, $\mathbf{R}_{17}^-$, $\mathbf{R}_{23}^-$ and $\mathbf{R}_{24}^-$,[73] it is possible to extrapolate electrophilicity values for CO$_2$ in the range from -15.3 to -18.7, while a value of -16.3 was reported according to a single experimental kinetic data with the indenide anion ($\mathbf{R}_2^-$)[37] (Table S8 in the ESI†). Many reports have discussed the theoretical prediction of nucleophilicity/electrophilicity.[48,74–76]

(iii) The variations of ΔG^0 and $\Delta G^{\ddagger}$ values for the carboxylation step represented in Fig. 2 are mainly related to enthalpic contributions, while the $T\Delta S^0$ and $T\Delta S^{\ddagger}$ terms are found to be almost constant in the carbanion series (Tables S4–S7 and Fig. S7 in the ESI†), with average values of -10.6 ± 0.8 and -9.95 ± 0.8 kcal mol^{-1}, respectively (the error is given as the standard deviation).

(iv) In the reactivity investigated, the formation of a reactant complex between the anion and carbon dioxide could in principle occur,[63,77] in particular for highly basic carbanions. Based on our calculations and IRC analysis, we do not have evidence for the formation of such a reactant complex; the calculated energy barriers refer then to the isolated reactants.

Distortion interaction analysis

We rationalised the molecular factors that impact the energetic barrier of the carboxylation step by employing the distortion/interaction model (also known as the activation/strain model) for bimolecular reactions, developed independently by the Bickelhaupt and Houk groups.[40] Accordingly, the potential energy ΔE along the reaction coordinate is given by the sum of

the energy due to the distortion of the reactants ($\Delta E_{\mathrm{distortion}} > 0$) and the energy given by the interaction of the two reactants ($\Delta E_{\mathrm{interaction}} < 0$), eqn (7).

$$\Delta E = \Delta E_{\mathrm{distortion}} + \Delta E_{\mathrm{interaction}} \tag{7}$$

Fig. 3A reports the ΔE *versus* the $\mathrm{C}(\mathbf{R}_i^-)\cdots\mathrm{C}(\mathrm{CO}_2)$ distance as the reaction coordinate for the carboxylation step of $\mathbf{R_3}^-$, $\mathbf{R_4}^-$,

$\mathbf{R_{17}}^-$, $\mathbf{R_{21}}^-$ and $\mathbf{R_{28}}^{2-}$ as representative cases, spanning the entire range of $\Delta G^{\ddagger}$ explored. As can be visually perceived, the profiles show a switch from a late to an early transition state along the series $\mathbf{R_{17}}^- \sim \mathbf{R_3}^- \rightarrow \mathbf{R_4}^- \rightarrow \mathbf{R_{21}}^- \rightarrow \mathbf{R_{28}}^{2-}$, consistent with the progressive decrease of activation energy. When the ΔE is dissected into the $\Delta E_{\mathrm{distortion}}$ and $\Delta E_{\mathrm{interaction}}$ contributions (Fig. 3B and Table S9 in the ESI†), the profiles suggest that the carboxylation step is both distortion- and interaction-controlled,[78,79] with an evident contribution from the interaction of the carbanions with CO_2.

According to energy decomposition analysis, with some software the $\Delta E_{\mathrm{interaction}}$ could be dissected into separate contributions from electrostatic interaction, Pauli repulsion, orbital interaction and dispersion interaction.[79] In the present case, the previous correlation between the activity and basicity of carbanions (Fig. 2B) identifies pK_{aH} as the physical parameter impacting the interaction. This is also supported by a smooth correlation between nucleophilicity and proton affinity among nucleophiles belonging to the same class.[75]

Concerning the distortion, the $\Delta E_{\mathrm{distortion}}$ can be decomposed into the contributions of the carbanion $\mathbf{R}_i^-$ and CO_2 reactants (eqn (8)); the $\Delta E_{\mathrm{distortion}}$ for each reactant along the reaction coordinate is given by the single point energy difference between the geometry of the reactant at each point and the geometry of the isolated reactant.[40,78,79]

$$\Delta E_{\mathrm{distortion}} = \Delta E_{\mathrm{distortion}}\,(\mathbf{R}_i^-) + \Delta E_{\mathrm{distortion}}\,(\mathrm{CO}_2) \tag{8}$$

Splitting the $\Delta E_{\mathrm{distortion}}$ along the reaction coordinate according to eqn (8) shows that the major energy penalty arises from CO_2 for the five cases investigated, Fig. 3C. Consistently, by expanding the analysis by evaluating the $\Delta E_{\mathrm{distortion}}\,(\mathbf{R}_i^-)$ and $\Delta E_{\mathrm{distortion}}\,(\mathrm{CO}_2)$ contributions with the transition state geometries of all $\mathbf{R}_i^-$ species, it is observed that the $\Delta E_{\mathrm{distortion}}$ of CO_2 exceeds the $\Delta E_{\mathrm{distortion}}$ of carbanions by *ca.* 5 times (Fig. S8 in the ESI;† note that for rigid "sp" carbanions such as $\mathbf{R_4}^-$ and $\mathbf{R_5}^-$ the $\Delta E_{\mathrm{distortion}}\,(\mathbf{R}_i^-)$ is almost negligible).

From a structural point of view, the distortion of carbon dioxide in the transition states is obviously described by the
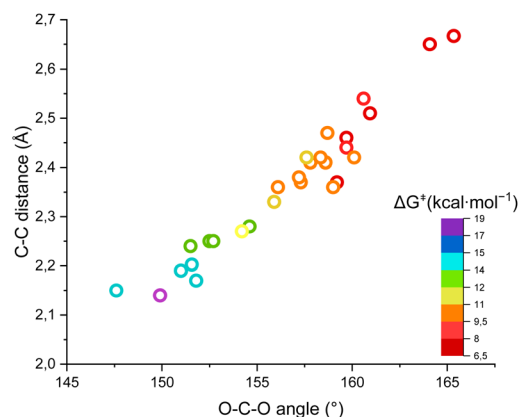

Fig. 3 (A) Plot of ΔE *vs.* the $\mathrm{C}(\mathbf{R}_i^-)\cdots\mathrm{C}(\mathrm{CO}_2)$ distance as the reaction coordinate for $\mathbf{R_3}^-$, $\mathbf{R_4}^-$, $\mathbf{R_{17}}^-$, $\mathbf{R_{21}}^-$ and $\mathbf{R_{28}}^{2-}$ as representative cases. (B) Dissection of ΔE into $\Delta E_{\mathrm{distortion}}$ and $\Delta E_{\mathrm{interaction}}$. (C) Dissection of $\Delta E_{\mathrm{distortion}}$ into $\Delta E_{\mathrm{distortion}}^{\ddagger}\,(\mathbf{R}_i^-)$ and $\Delta E_{\mathrm{distortion}}^{\ddagger}\,(\mathrm{CO}_2)$. In all graphs, the empty dots indicate the transition states.

Fig. 4 Plot of the $\Delta G^{\ddagger}$ for the carboxylation of the carbanions *versus* the O–C–O angle and the $\mathrm{C}(\mathbf{R}_i^-)\cdots\mathrm{C}(\mathrm{CO}_2)$ distance in the transition states.

bending of CO_2 and by the contraction of the O–C–O angle, while the carbanion nucleophile approaches and the $C(\mathbf{R}_i^-)\cdots C(CO_2)$ distance decreases. Calculations show indeed a linear trend in the carbanion series between the $\Delta G^{\ddagger}$ of carboxylation and the O–C–O angle (see Fig. S9 in the ESI†), predicting that one kcal mol^{-1} of penalty in the $\Delta G^{\ddagger}$ is associated with a decrease of $1.41 \pm 0.09°$ of the O–C–O angle in the transition state.

Fig. 4 shows the $\Delta G^{\ddagger}$, the O–C–O angle and the C···C distance in a single graph, demonstrating that the higher the free energy of activation, the higher the required distortion of CO_2 in a "late" transition state, with a small O–C–O angle and a short $C(\mathbf{R}_i^-)\cdots C(CO_2)$ distance.

Conclusions and perspectives

In conclusion, we have reported energy and structural correlations for the carboxylation step of carbanions with CO_2. These allow linking the basicity of the carbanion (pK_{aH}), the standard and activation free energies of the carboxylation step (ΔG^0 and $\Delta G^{\ddagger}$) and the distortion of CO_2 in the transition state (O–C–O angle and $C(\mathbf{R}_i^-)\cdots C(CO_2)$ distance), deriving reactivity descriptors such as the Leffler–Hammond coefficient, the intrinsic barrier and the electrophilicity of CO_2.

These tools are instrumental for the design of experimental chemical, electrochemical or photochemical fixation of CO_2 into organic compounds. The *a priori* evaluation of the reaction barrier (and consequently the rate constant) between a carbanion and CO_2 should be pivotal in driving the envisaged carboxylation reactivity with respect to undesired competitive pathways. In particular, these may include irreversible protonation of the carbanion or its reactivity with other electrophiles (as documented in the case of electrochemical carboxylation of α,β-unsaturated ketones[57]). The regioselectivity of the carboxylation step could also be a challenge and should be considered when involving extended organic scaffolds, as in the case of electrochemical carboxylation of dienes[80] and naphthalene derivatives.[81] Thus, we hope to provide a guide for future studies on carbon dioxide reconversion.

Data availability

The data supporting this article have been included as part of the ESI.†

Author contributions

All authors conceptualised the research and contributed to the discussion of the results. C. N., M. O. and A. S. performed the calculations. C. N. and A. S. co-wrote the manuscript. L. D. A. and A. S. were responsible for funding acquisition.

Conflicts of interest

There are no conflicts to declare.

Notes and references

1 (*a*) D. I. A. McKay, A. Staal, J. F. Abrams, R. Winkelmann, B. Sakschewski, S. Loriani, I. Fetzer, S. E. Cornell, J. Rockström and T. M. Lenton, *Science*, 2022, **377**, eabn7950; (*b*) S. I. Zandalinas, F. B. Fritschi and R. Mittler, *Trends Plant Sci.*, 2021, **26**, 588–599.

2 (*a*) IEA International Energy Agency, Carbon Capture, Utilisation and Storage, https://www.iea.org/energy-system/carbon-capture-utilisation-and-storage; (*b*) K. Kohse-Höinghaus, *Chem. Rev.*, 2023, **123**, 5139–5219; (*c*) P. Friedlingstein, M. O. Sullivan, *et al.*, *Earth Syst. Sci. Data*, 2023, **15**, 5301–5369; (*d*) L. Chen, G. Msigwa, M. Yang, A. I. Osman, S. Fawzy, D. W. Rooney and P.-S. Yap, *Environ. Chem. Lett.*, 2022, **20**, 2277–2310.

3 United Nations 17, Sustainable Development Goals, https://www.un.org/sustainabledevelopment/.

4 (*a*) T. L. Biel-Nielsen, T. A. Hatton, S. N. B. Villadsen, J. S. Jakobsen, J. L. Bonde, A. M. Spormann and P. L. Fosbøl, *ChemSusChem*, 2023, e202202345; (*b*) R. J. Detz, C. J. Ferchaud, A. J. Kalkman, J. Kemper, C. Sanchez-Martinez, M. Saric and M. V. Shinde, *Sustainable Energy Fuels*, 2023, **7**, 5445–5472.

5 K. M. Diederichsen, R. Sharifian, J. S. Kang, Y. Liu, S. Kim, B. M. Gallant, D. Vermaas and T. A. Hatton, *Nat. Rev. Methods Primers*, 2022, **2**, 68.

6 A. Hasanzadeh, S. Ghazanfari, M. Janbazvatan, H. Rashidpour, A. Chitsaz and M. Khalilian, *J. CO_2 Util.*, 2023, **67**, 102306.

7 J. Albero, Y. Peng and H. García, *ACS Catal.*, 2020, **10**, 5734–5749.

8 B. Chang, H. Pang, F. Raziq, S. Wang, K.-W. Huang, J. Ye and H. Zhang, *Energy Environ. Sci.*, 2023, **16**, 4714–4758.

9 S. Fang, M. Rahaman, J. Bharti, E. Reisner, M. Robert, G. A. Ozin and Y. H. Hu, *Nat. Rev. Methods Primers*, 2023, **3**, 61.

10 S. Ren, D. Joulié, D. Salvatore, K. Torbensen, M. Wang, M. Robert and C. P. Berlinguette, *Science*, 2019, **365**, 367–369.

11 Q. Zhu, X. Sun, D. Yang, J. Ma, X. Kang, L. Zheng, J. Zhang, Z. Wu and B. Han, *Nat. Commun.*, 2019, **10**, 3851.

12 M. Han, X. Fu, A. Cao, C. Guo, W. Chu and J. Xiao, *Adv. Theory Simul.*, 2019, **2**, 1800200.

13 Q. Liu, L. Wu, R. Jackstell and M. Beller, *Nat. Commun.*, 2015, **6**, 5933.

14 Q. W. Song, R. Ma, P. Liu, K. Zhang and L. N. He, *Green Chem.*, 2023, **25**, 6538–6560.

15 S. Pimparkar, A. K. Dalvi, A. Koodan, S. Maiti, S. A. Al-Thabaiti, M. Mokhtar, A. Dutta, Y. R. Lee and D. Maiti, *Green Chem.*, 2021, **23**, 9283–9317.

16 S. Bierbaumer, M. Nattermann, L. Schulz, R. Zschoche, T. J. Erb, C. K. Winkler, M. Tinzl and S. M. Glueck, *Chem. Rev.*, 2023, **123**, 5702–5754.

17 M. M. F. Hasan, L. M. Rossi, D. P. Debecker, K. C. Leonard, Z. Li, B. C. E. Makhubela, C. Zhao and A. Kleij, *ACS Sustainable Chem. Eng.*, 2021, **9**, 12427–12430.

18 P. K. Sahoo, Y. Zhang and S. Das, *ACS Catal.*, 2021, **11**, 3414–3442.

19 J. Ding, R. Ye, Y. Fu, Y. He, Y. Wu, Y. Zhang, Q. Zhong, H. H. Kung and M. Fan, *Nat. Commun.*, 2023, **14**, 4586.

20 H. Kolbe, *Adv. Cycloaddit.*, 1860, **113**, 125–127.

21 R. Schmitt, *J. Prakt. Chem.*, 1885, **2**, 397–410.

22 A. Tortajada, F. Juliá-Hernández, M. Börjesson, T. Moragas and R. Martin, *Angew. Chem., Int. Ed.*, 2018, **57**, 15948–15982.

23 J. Davies, J. R. Lyonnet, B. Carvalho, B. Sahoo, C. S. Day, F. Juliá-Hernández, Y. Duan, N. Álvaro Velasco-Rubio, M. Obst, P. O. Norrby, K. H. Hopmann and R. Martin, *J. Am. Chem. Soc.*, 2024, **146**, 1753–1759.

24 C. Qiao, W. Shi, A. Brandolese, J. Benet-Buchholz, E. C. Escudero-Adán and A. W. Kleij, *Angew. Chem., Int. Ed.*, 2022, **61**, e202205053.

25 Y. Yan, J. Hao, F. Xie, F. Han, L. Jing and P. Han, *J. Org. Chem.*, 2023, **88**, 14640–14648.

26 S. Zheng, T. Zhang and H. Maekawa, *J. Org. Chem.*, 2022, **87**, 7342–7349.

27 J. Wang, Z. F. Wei, Y. X. Luo, C. H. Lu and R. J. Song, *SynOpen*, 2024, **8**, 116–124.

28 H. Senboku, *Chem. Rec.*, 2021, **21**, 2354–2374.

29 P. Franceschi, E. Rossin, G. Goti, A. Scopano, A. Vega-Penaloza, M. Natali, D. Singh, A. Sartorel and L. Dell'Amico, *J. Org. Chem.*, 2023, **88**, 6454–6464.

30 M. Schmalzbauer, T. D. Svejstrup, F. Fricke, P. Brandt, M. J. Johansson, G. Bergonzini and B. König, *Chem*, 2020, **6**, 2658–2672.

31 Z. Zhang, J. H. Ye, T. Ju, L. L. Liao, H. Huang, Y. Y. Gui, W. J. Zhou and D. G. Yu, *ACS Catal.*, 2020, **10**, 10871–10885.

32 H. Seo, M. H. Katcher and T. F. Jamison, *Nat. Chem.*, 2017, **9**, 453–456.

33 Y. Naito, Y. Nakamura, N. Shida, H. Senboku, K. Tanaka and M. Atobe, *J. Org. Chem.*, 2021, **86**, 15953–15960.

34 A. Sheta, A. Alkayal, M. Mashaly, S. Said, S. Elmorsy, A. V Malkov and B. R. Buckley, *Angew. Chem., Int. Ed.*, 2021, **60**, 21832–21837.

35 Q. Y. Meng, T. E. Schirmer, A. L. Berger, K. Donabauer and B. König, *J. Am. Chem. Soc.*, 2019, **141**, 11393–11397.

36 K. M. Waldie, A. L. Ostericher, M. H. Reineke, A. F. Sasayama and C. P. Kubiak, *ACS Catal.*, 2018, **8**, 1313–1324.

37 Z. Li, R. J. Mayer, A. R. Ofial and H. Mayr, *J. Am. Chem. Soc.*, 2020, **142**, 8383–8402.

38 F. G. Bordwell and D. L. Hughes, *J. Org. Chem.*, 1980, **45**, 3314–3320.

39 H. Mayr and A. R. Ofial, *Acc. Chem. Res.*, 2016, **49**, 952–965.

40 F. M. Bickelhaupt and K. N. Houk, *Angew. Chem., Int. Ed.*, 2017, **56**, 10070–10086.

41 M. J. Frisch, G. W. Trucks, H. B. Schlegel, G. E. Scuseria, M. A. Robb, J. R. Cheeseman, G. Scalmani, V. Barone, G. A. Petersson, H. Nakatsuji, X. Li, M. Caricato, A. V. Marenich, J. Bloino, B. G. Janesko, R. Gomperts, B. Mennucci, H. P. Hratchian, J. V. Ortiz, A. F. Izmaylov, J. L. Sonnenberg, D. Williams-Young, F. Ding, F. Lipparini, F. Egidi, J. Goings, B. Peng, A. Petrone, T. Henderson, D. Ranasinghe, V. G. Zakrzewski, J. Gao, N. Rega, G. Zheng, W. Liang, M. Hada, M. Ehara, K. Toyota, R. Fukuda, J. Hasegawa, M. Ishida, T. Nakajima, Y. Honda, O. Kitao, H. Nakai, T. Vreven, K. Throssell, J. A. Montgomery Jr, J. E. Peralta, F. Ogliaro, M. J. Bearpark, J. J. Heyd, E. N. Brothers, K. N. Kudin, V. N. Staroverov, T. A. Keith, R. Kobayashi, J. Normand, K. Raghavachari, A. P. Rendell, J. C. Burant, S. S. Iyengar, J. Tomasi, M. Cossi, J. M. Millam, M. Klene, C. Adamo, R. Cammi, J. W. Ochterski, R. L. Martin, K. Morokuma, O. Farkas, J. B. Foresman, and D. J. Fox, *Gaussian 16, Revision C.01*, Gaussian, Inc., Wallingford CT, 2016.

42 J. J. P. Stewart, *J. Comput. Chem.*, 1989, **10**, 209–220.

43 J. J. P. Stewart, *J. Comput. Chem.*, 1989, **10**, 221–264.

44 E. Anders, R. Koch and P. Freunscht, *J. Comput. Chem.*, 1993, **14**, 1301–1312.

45 S. Miertuš, E. Scrocco and J. Tomasi, *Chem. Phys.*, 1981, **55**, 117–129.

46 S. Miertuš and J. Tomasi, *Chem. Phys.*, 1982, **65**, 239–245.

47 J. L. Pascual-Ahuir, E. Silla and I. Tuñón, *J. Comput. Chem.*, 1994, **15**, 1127–1138.

48 J. N. Harvey, F. Himo, F. Maseras and L. Perrin, *ACS Catal.*, 2019, **9**, 6803–6813.

49 R. F. Ribeiro, A. V. Marenich, C. J. Cramer and D. G. Truhlar, *J. Phys. Chem. B*, 2011, **115**, 14556–14562.

50 J. Da Chai and M. Head-Gordon, *Phys. Chem. Chem. Phys.*, 2008, **10**, 6615–6620.

51 A. Schäfer, H. Horn and R. Ahlrichs, *J. Chem. Phys.*, 1992, **97**, 2571–2577.

52 F. Weigend, *Phys. Chem. Chem. Phys.*, 2006, **8**, 1057–1065.

53 R. A. Kendall, T. H. Dunning and R. J. Harrison, *J. Chem. Phys.*, 1992, **96**, 6796–6806.

54 D. E. Woon and T. H. Dunning, *J. Chem. Phys.*, 1993, **98**, 1358–1371.

55 T. Schwabe and S. Grimme, *Phys. Chem. Chem. Phys.*, 2007, **9**, 3397–3406.

56 J. A. Pople, P. M. W. Gill and B. G. Johnson, *Chem. Phys. Lett.*, 1992, **199**, 557–560.

57 P. Franceschi, C. Nicoletti, R. Bonetto, M. Bonchio, M. Natali, L. Dell'Amico and A. Sartorel, *Front. Chem.*, 2021, **9**, 783993.

58 O. Larrañaga, A. De Cõzar, F. M. Bickelhaupt, R. Zangi and F. P. Cossío, *Chem.–Eur. J.*, 2013, **19**, 13761–13773.

59 F. Bordwell, W. J. J. Boyle, J. A. Hautala and K. C. Yee, *J. Am. Chem. Soc.*, 1969, **91**, 4002–4003.

60 S. Zhou, Y. Wang and J. Gao, *JACS Au*, 2021, **1**, 233–244.

61 Y. Fu, X. Suo, Z. Yang, S. Dai and D. E. Jiang, *J. Phys. Chem. B*, 2022, **126**, 6979–6984.

62 F. M. Bickelhaupt and I. Fernández, *Chem. Sci.*, 2024, **15**, 3980–3987.

63 D. Kong, P. J. Moon, E. K. J. Lui, O. Bsharat and R. J. Lundgren, *Science*, 2020, **369**, 557–561.

64 G. Destro, K. Horkka, O. Loreau, D. A. Buisson, L. Kingston, A. Del Vecchio, M. Schou, C. S. Elmore, F. Taran, T. Cantat and D. Audisio, *Angew. Chem., Int. Ed.*, 2020, **59**, 13490–13495.

65 H. Mayr, M. Breugst and A. R. Ofial, *Angew. Chem., Int. Ed.*, 2011, **50**, 6470–6505.

66 S. Hoz, H. Basch, J. L. Wolk, T. Hoz and E. Rozental, *J. Am. Chem. Soc.*, 1999, **121**, 7724–7725.

67 J. P. Richard, T. L. Amyes and M. M. Toteva, *Acc. Chem. Res.*, 2001, **34**, 981–988.

68 A. Kresge, *Acc. Chem. Res.*, 1975, **8**, 354–360.

69 C. R. Reinhardt, T. C. Jaglinski, A. M. Kastenschmidt, E. H. Song, A. K. Gross, A. J. Krause, J. M. Gollmar, K. J. Meise, Z. S. Stenerson, T. J. Weibel, A. Dison, M. R. Finnegan, D. S. Griesi, M. D. Heltne, T. G. Hughes, C. D. Hunt, K. A. Jansen, A. H. Xiong, S. Hati and S. Bhattacharyya, *J. Mol. Model.*, 2016, **22**, 199.

70 C. F. Bernasconi and P. J. Wenzel, *J. Am. Chem. Soc.*, 2001, **123**, 7146–7153.

71 Bordwell pKa table, collected by prof. Hans Reich (UW-Madison)**https://organicchemistrydata.org/hansreich/resources/pka/**last update April 2024.

72 H. Mayr and M. Patz, *Angew. Chem., Int. Ed.*, 1994, **33**, 938–957.

73 H. Mayr and A. R. Ofial, Mayr's Database of Reactivity Parameters, **https://www.cup.lmu.de/oc/mayr/reaktionsdatenbank2/**.

74 C. Wang, Y. Fu, Q. X. Guo and L. Liu, *Chem.–Eur. J.*, 2010, **16**, 2586–2598.

75 M. Orlandi, M. Escudero-Casao and G. Licini, *J. Org. Chem.*, 2021, **86**, 3555–3564.

76 M. Vahl and J. Proppe, *Phys. Chem. Chem. Phys.*, 2023, **25**, 2717–2728.

77 M. A. Zambri and R. Kluger, *J. Am. Chem. Soc.*, 2024, **146**, 1403–1409.

78 I. Fernández and F. M. Bickelhaupt, *Chem. Soc. Rev.*, 2014, **43**, 4953–4967.

79 P. Vermeeren, S. C. C. van der Lubbe, C. Fonseca Guerra, F. M. Bickelhaupt and T. A. Hamlin, *Nat. Protoc.*, 2020, **15**, 649–667.

80 A. M. Sheta, M. A. Mashaly, S. B. Said, S. S. Elmorsy, A. V Malkov and B. R. Buckley, *Chem. Sci.*, 2020, **11**, 9109–9114.

81 V. K. Rawat, H. Hayashi, H. Katsuyama, S. R. Mangaonkar and T. Mita, *Org. Lett.*, 2023, **25**, 4231–4235.